DOI: 10.1002/ejic.201000479

Structure and Metal-to-Insulator Transition of VO_2 Nanowires Grown on Sapphire Substrates

Yao Cheng,[a] Ting Zhang,[a] Yuan Cai,[a] Kin Ming Ho,[a] Kwok Kwong Fung,[a] and Ning Wang*[a]

Keywords: Metal-to-insulator transitions / Nanowires / Phase transitions / Chemical vapor deposition / Vanadium

Single-crystalline VO_2 nanowires exhibit interesting growth phenomena along three equivalent $<1\bar{1}00>$ directions of the C-planes of the sapphire substrates. Under certain growth conditions, VO_2 nanowires form V-shaped twining structures with uniform morphologies and interfaces. Due to the strong elastic stress at the interfaces, the metal-to-insulator transition (MIT) of individual VO_2 nanowires grown directly on sapphire substrates were observed to display distinct electrical hysteresis loops relative to VO_2 nanowires dispersed on sapphire substrates. The distinctive characteristics in the hysteresis loops, exhibited in the process of MIT, are shown to be correlated with the nucleation and growth of periodic/random domain structures in the nanowires during the heating and cooling processes. The periodic domain structures observed in the directly grown nanowires can be explained under the framework of a modified stress-induced elastic energy model that was first developed for ferroelectric systems.

Introduction

Vanadium dioxide (VO_2) is a material well known for its metal-to-insulator transition (MIT) accompanied by a reversible structural transition from a high-temperature tetragonal (T) phase to a low-temperature monoclinic (M) phase at 340 K.[1–6] This transition makes VO_2 a potentially useful material for applications in electrical and optical switching devices. In recent years, a tremendous impetus to materials applications has arisen from the ability to fabricate nanowire arrays with controlled crystalline structures and alignment. Various synthesis methods, including the vapor transport technique using metal catalysts, chemical solution syntheses, electric-field-assisted assembly techniques, and electrochemical fabrication based on anodic aluminum oxide templates, have been actively developed.[7–15] In this context, growth of nanowires directly on substrates provides an ideal way to control the properties and integration of the nanowire structures for technological applications. For VO_2 thin films, enormous strains exist at the interfaces, mainly due to the differences in the crystal lattice parameters and thermal expansion coefficients between the thin film and the substrate.[16,17] The stress is particularly significant during the phase transformation and may influence the properties of the thin films. It follows that VO_2 nanowires grown along sapphire substrate surfaces may exhibit interesting growth features, although there has been a dearth of studies on the interface stress/structures and their influence on the MIT transition of the VO_2 nanowires.

In this work, we report on the structural characterization of single-crystalline VO_2 nanowires grown on the C-planes of sapphire substrates by thermal evaporation. The MIT characteristics of individual VO_2 nanowires were studied in comparison with the reference system – nanowires lying flat on the substrate, prepared by a dispersion method. We observed that all VO_2 nanowires grew along specific directions with uniform morphology and interfacial structures. Due to the strong elastic interfacial stress, VO_2 nanowires show a significant shift in the electrical hysteresis loops and exhibit a broader temperature range for the MIT process. By using a modified stress-induced elastic energy model, we correlate and explain the hysteresis behavior observed during the MIT process with the formation and growth of periodic domain structures.

Results and Discussion

Figure 1A is a SEM image showing the typical morphology of as-grown VO_2 nanowires formed on a (0001) sapphire substrate at 900 °C. Under our experimental conditions, all VO_2 nanowires grew along the three equivalent $<1\bar{1}00>$ directions. The diameters of these nanowires were about 100–300 nm, and their lengths were from several to tens of micrometers. The inset in Figure 1A is the histogram of VO_2 nanowire size distribution. The angles between the nanowires were 60°, 120°, or they were parallel to each other. Obviously, the $<1\bar{1}00>$ direction on the (0001) sap-

[a] Department of Physics and the William Mong Institute of Nano Science & Technology, The Hong Kong University of Science and Technology,
Hong Kong, China
E-mail: phwang@ust.hk

phire substrate is the preferential growth direction of VO_2 nanowires. In addition, at the temperature range from 800 to 850 °C, almost all VO_2 nanowires formed V-shaped structures with a fixed angle of 120° (see Figure 1B). All these V-shaped nanowires had similar morphologies, that is, their growth direction, cross-section, and crystalline structure were similar to those formed at 900 °C. As illustrated in the enlarged picture in the inset of Figure 1B, most of the V-shaped nanostructures had a clear boundary between their two branches. We observed a number of VO_2 nanowires by TEM. As shown in Figure 1C, all nanowires have uniform diameters and flat side surfaces (see also Figure 1D). The growth front of the VO_2 nanowire shown in Figure 1E is very clear. No catalyst is observed. Similar to the growth of VO_2 nanowires we investigated previously, we believe that the VO_2 nanowires formed under our experimental conditions could be growing under the oxide-assisted mechanism.[18] So far, the growth mechanisms of VO_2 nanowires are still poorly understood, and controversial mechanisms of vapor–solid growth have been proposed.[1,19]

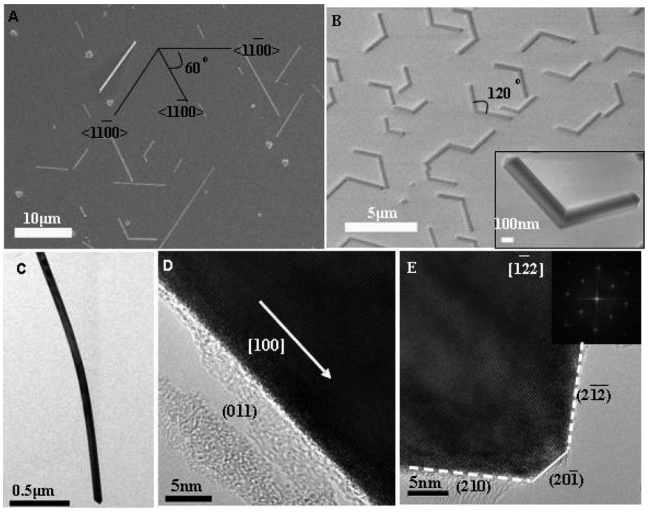

Figure 1. (A, B) SEM images of the VO_2 nanowires grown along the three equivalent <1$\bar{1}$00> directions of the C-plane. The inset in (A) is the histogram of VO_2 nanowire size distribution. In the temperature range from 800 to 850 °C, almost all VO_2 nanowires formed V-shaped structures. (C) A TEM image showing the typical uniform morphology of VO_2 nanowires; (D and E) atomic structures of a nanowire side surface and growth front, respectively.

By sectioning the nanowire samples, we observed that all VO_2 nanowires exhibited a triangular cross-section with specific growth directions and crystal orientations with respect to the substrate. Figure 2A presents a typical cross-sectional TEM image of a VO_2 nanowire grown along the substrate surface. Figure 2B illustrates the atomic structure at the interface of the substrate. According to the high-resolution TEM (HRTEM) image (Figure 2B) and the Fourier transform (FFT) patterns, we concluded that the nanowires grew along the [100] direction of the monoclinic VO_2, while the (011) and (01$\bar{1}$) planes were parallel to the side facets. The orientation relationship between the VO_2 nanowires and the sapphire substrate can be described as $(020)_{VO2}$// $(0002)_{sapphire}$ and $[100]_{VO2}$//$[<1\bar{1}00]_{sapphire}$. Different from the growth direction (along <11$\bar{2}$0>) of the VO_2 nanowires observed by Sohn et al.,[1] the nanowires shown in this work always grew along the three equivalent <1$\bar{1}$00> directions. We have identified that compressive strain exists at the interface between the VO_2 nanowires and the substrate. On the C-plane of a sapphire substrate, the lattice plane spacing, or *d*-spacing, of $(110)_{Al2O3}$ is about 0.238 nm. For the low-temperature VO_2 phase, the *d*-spacing of $(101)_{VO2}$ is about 0.4554 nm. As shown in Figure 2B, at the interface, 19 $(110)_{Al2O3}$ planes (19 × 0.238 = 4.522 nm) match 10 $(001)_{VO2(M)}$ planes (10 × 0.48464 = 4.8464 nm). The VO_2 nanowire should be in compressive strain. This is very reasonable, because VO_2 nanowires are formed at a high temperature, at which the nanowires should be in the metallic phase (tetragonal structure). Then, the interface is actually along the (010) of the tetragonal phase. The *d*-spacing of $(010)_{VO2(T)}$ is about 0.4554 nm, and 10 $(010)_{VO2(T)}$ equals 4.554 nm, which matches fairly well with the value for the 19 $(110)_{Al2O3}$ planes. In the high-temperature phase of tetragonal VO_2, each vanadium atom is surrounded by a distorted octahedron of oxygen atoms, and the $(100)_T$ planes have a similar arrangement and interatomic spacing as the closely packed oxygen lattice in the (0001) plane of the sapphire substrate.[20–22] VO_2 nanowires tend to grow along the $[100]_M$ direction as observed on various substrates, for example, sapphire, silica, and Si_3N_4.[1,19,23,24] Therefore, the lattice match between the high-temperature VO_2 tetragonal structure and the sapphire (0001) surface suggests that the <1$\bar{1}$00> preferred growth direction of the nanowires is along the direction of sapphire.

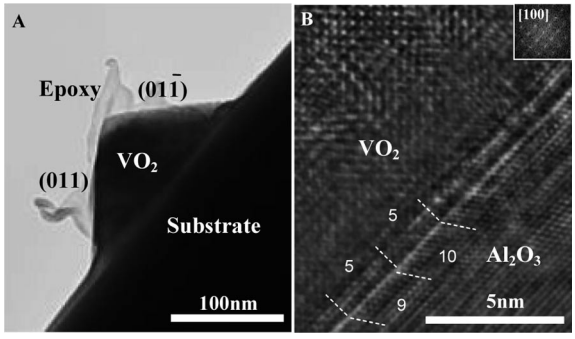

Figure 2. (A) A cross-sectional TEM image of a single VO_2 nanowire grown on a sapphire substrate with its (011) and (01$\bar{1}$) surfaces parallel to the nanowire axis. (B) An HRTEM image showing the interface structure and its corresponding FFT patterns (inset) to confirm the orientation relationship between the nanowire and the substrate.

The V-shaped VO_2 nanowires (Figures 3A, B) have a very similar growth direction and shape relative to the single nanowires. The junction of the two-branch wires is a flat twin boundary, as illustrated by the electron diffraction pattern in Figure 3C and the HRTEM image in Figure 3D. However, a very thin space at the boundary often exists in some V-shaped nanowires (see Figures 3B, E). On the basis of our study, we believe that the formation of the V-shaped nanowires is due to the formation of twining structures of

VO_2 crystals (Figure 3D). This kind of twining is more likely formed when the growth temperature is lowered during the initial growth of the nanowires.

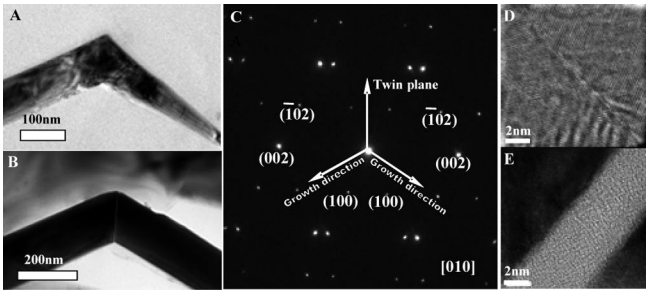

Figure 3. (A) and (B) are plane-view images of the V-shaped bicrystalline VO_2 nanostructures grown on the C-plane of a sapphire substrate. (B) A thin space along the twin boundary has been observed in some V-shaped nanostructures. (C) A SAED pattern recorded from the boundary area can be indexed as the twin structure of monoclinic VO_2. (D) and (E) are the HRTEM images of the twin boundary with or without the space.

To investigate the electrical transport properties of VO_2 nanowires during the structural transition, we fabricated two different types of VO_2 nanowire devices: (i) "dispersed devices" based on the nanowires simply dispersed on the C-plane sapphire substrate; and (ii) "grown devices" based on the nanowires grown directly on the C-plane sapphire substrate. As shown in Figure 4A, the curve depicting the change in resistance as a function of temperature (r.t.) of the "dispersed devices" followed a typical four-terminal configuration. This curve shows the electrical switching from a monoclinic, high-resistance insulating state to a tetragonal, low-resistance metallic state, and the switching occurs at a higher temperature on the upsweep than on the downsweep. A dramatic change in the resistance [about 4 orders (10^4) of magnitude] in the device has been observed, and the electrical switching was completed at 92 °C. During the heating and/or cooling cycles, some steps (labeled as I to V in Figure 4A) appeared on the resistance curve over a much wider temperature range, especially during the downsweep process. This phenomenon has not been observed in bulk VO_2 materials. As shown in Figure 4B, the grown devices show noticeably different r.t. behavior during the heating and cooling cycles. Some little steps were also observed over a wider temperature range during the electrical switching loops. We found that the electrical switching was completed at about 122 °C, which was much higher than the value for the "dispersed devices". The electrical hysteresis loop shifted to the high-temperature region when the nanowire was grown on the substrate, and the transition temperature range was also much broader than that for the dispersed devices. We have measured more than ten nanowire devices and the results were repeated. The detailed shapes of the hysteresis loops depend on the individual nanowires; however, the final transition temperature was always around 122(±1) °C.

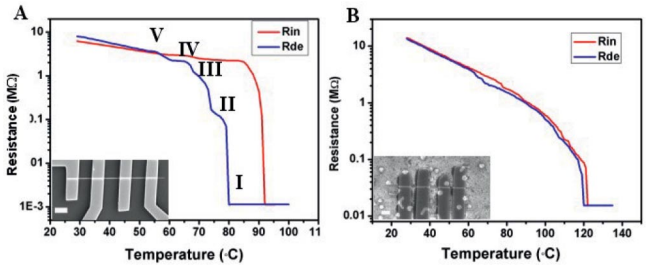

Figure 4. (A) Changes in the resistance as a function of temperature, measured by four-probe geometry, of a VO_2 nanowire dispersed on the substrate. (B) Similar measurements of the resistance changes of a nanowire grown on the substrate. The red and blue curves indicate heating and cooling, respectively. The insets are SEM images of the nanowire devices. The scale bar in the SEM images is 1 μm.

In this study, we have observed interesting evolutionary processes in the formation and growth of domain structures in different types of VO_2 nanowires during MIT. In dispersed VO_2 nanowires, Figure 5A shows optical microscope images of the formation and shape changes of the domains during heating and cooling processes. Initially, the domains of the high-temperature phase nucleated randomly along the nanowires and grew continuously with increasing temperature. At about 90 °C, the nanowires transformed almost completely to the high-temperature phase. Because the resistance of the nanowires was determined mainly by the short monoclinic phase, the final phase transition caused a dramatic drop in the resistance, as shown in Figure 4A.

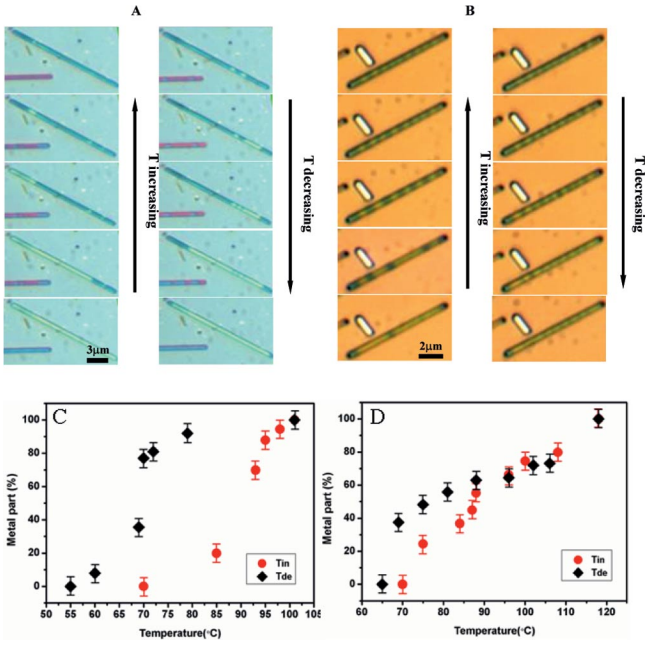

Figure 5. The optical images showing changes in the domain patterns in VO_2 nanowires (A) dispersed on the substrate and (B) grown on the substrate during heating and cooling processes. The dark contrast indicates the domains of the high-temperature tetragonal structure. (C) and (D) are the variation of the percentages of the metallic phases as a function of temperature for the cases (A) and (B) respectively. "Tin" and "Tde" represent temperature increasing and decreasing processes, respectively.

During the cooling process, totally different domains of the low-temperature phase randomly appeared. Some large domains appeared and segregated quickly as the temperature decreased. This transition process therefore induced some steps in the r.t. curve during cooling, as observed in Figure 4A. Because the transition process depends on the individual nanowire structures, the electrical properties measured in different nanowires have slightly different features.

In the nanowires grown on the substrate, we observed different nucleation and growth behaviors in the domain structure. The domains formed more periodically, and their number increased with increasing temperature (see Figure 5B). New domains appeared at certain positions so that the domains were equally spaced along the nanowires. In the mean time, the space between the newly formed domains decreased. Eventually, the nanowire became a single domain in the high-temperature phase. When the temperature decreased, however, the reverse MIT transition showed distinct features. First, periodic domains appeared quickly at about 95 to 100 °C. Then, the number of domains remained constant, but the size of each domain shrank as the temperature decreased until the transition was totally completed. Figures 5C and D show the variation of the percentages of the metallic phases as a function of temperature for the cases of Figures 5A and B, respectively. For different sizes of VO_2 nanowires, we have found that the domain size is diameter-dependent, that is, at the same temperature, the thicker the nanowires, the larger the domain period.

Periodic domain structures have been observed in VO_2 nanobeams,[23] strained ferroelectrics,[25–27] bulk VO_2 single crystals,[28–31] and magnetoresistive complex oxides.[32] By considering the effect of microstresses at the nanowire interfaces, Wu et al.[23] demonstrated that the uniformly distributed interface strain on VO_2 nanowires may result in periodic domain patterns during MIT. In our analysis, however, we consider both micro- and macrostress parts inside the free energy expression. This is because if there is no macrostress part inside the free energy expression (see our analysis below), the system should not have an energy minimum via the percentage of the metallic phase. The phase transition in VO_2 has been determined to originate from the tilting and shifting of the cation–cation pairs along the *a*- or the *c*-axes (the growth direction of our VO_2 nanowires). In order to realize the transition from monoclinic to tetragonal structures,[33] the uniaxial strain can easily appear along the growth direction of the nanowires. Under the framework of a modified stress-induced elastic energy model that was first developed for ferroelectric systems,[27,34] the formation of periodic domain structures observed in VO_2 nanowires during temperature increase and decrease may be explained. The formation of periodic domain structures during the phase transformation in heterostructures can be attributed to the minimization of the free energy of the system, which consists of misfit elastic energy and domain wall energy, etc. Applying these concepts to our case, after some simple derivation we can estimate the free energy of the two-phase VO_2 nanowires grown on the substrate during MIT.

$$F = h\{(1-\alpha)[f_{\text{Insulator}}(T) + e_{\text{Insulator}}] + \alpha[f^0{}_{\text{Metallic}}(T) + e_{\text{Metallic}}] - \alpha(1-\alpha)(1-\eta)e^I\} + \xi\alpha^2(1-\alpha)^2De^I + 2\gamma h/D + \Gamma_0 \quad (1)$$

In Equation (1), F is the free enery of the system per unit nanowire/substrate interface area, h is the nanowire thickness, and α is the ratio of metallic phase in the domain length. The variables $f_{\text{Insulator}}(T)$ and $f_{\text{Metallic}}(T)$ denote the free energy densities of the insulator and metallic phases of the VO_2 bulk material, and they are functions of temperature; $e_{\text{Insulator}}$ and e_{Metallic} are elastic energy densities due to the misfit between the insulator or metallic phase and the substrate; e^I is the elastic energy density due to misfit between metallic and insulator phase; η and ξ are constants with magnitudes of 1.[27,34] D is the spatial period of the domain pattern, γ is the domain-wall energy areal density, and Γ_0 is the areal energy density of the interface between VO_2 nanowire and substrate.

Analyzing the free energy expression, we can derive the equilibrium domain period, D_0, and the percentage of metallic phase, α_0, in the domain structure under a certain temperature, by using the condition $\frac{\partial F}{\partial D} = 0$, $\frac{\partial F}{\partial \alpha} = 0$, and $\frac{\partial^2 F}{\partial \alpha^2} > 0$.

$$\alpha_0 = \frac{1}{2} + \frac{h(f_{\text{Insulator}}(T) - f_{\text{Metallic}}(T) + e_{\text{Insulator}} - e_{\text{Metallic}})}{2[h(1-\eta)e^I - 2\sqrt{2\gamma h\xi e^I}]} \quad (2)$$

$$D_0 = \sqrt{\frac{2\gamma h}{\xi e^I}} \frac{1}{\alpha_0(1-\alpha_0)} \quad (3)$$

$$(1-\eta)\sqrt{he^I} > 2\sqrt{2\gamma\xi} \quad (4)$$

With these equations, we can see that there should be one free energy minimum for one temperature (since free energy density of the bulk VO_2 metal or insulator phase are both functions of temperature), and the corresponding equilibrium domain period and metal phase percentage in the nanowires are given by Equations (2) and (3). The free energy densities $f_{Insulator}(T)$ and $f_{Metallic}(T)$ are coarsely linear with temperature, and obviously the quantity $f_{Insulator}(T) - f_{Metallic}(T)$ changes sign during the phase-transition process, when the temperature changes. Therefore, these equations show that, as a phase-transition process goes from one pure phase, A, at temperature T(A), to the other pure phase, B, at temperature T(B), the period of polydomain structure, D_0, decreases from infinity (pure phase A, $\alpha_0 = 0$) to a minimum value of $D_0 = 4\sqrt{2\gamma h/\xi e^I}$ (corresponding to $\alpha_0 = 0.5$) and then increases again to infinity (pure phase B, $\alpha_0 = 1$). This fact can explain the formation and variation of the periodic polydomain structure

of grown nanowires in a phase-transition process. In Figure 5 we can clearly see the change in domain period and metallic phase percentage both in the heating and cooling processes. However, the present analysis is not able to fully explain the interesting hysteresis behavior that was observed in the heating and cooling processes, in which domain period D_0 seems to change more significantly during the heating process while metallic phase percentage a_0 changes more significantly during cooling. This difference in behavior exists even at the same temperature, thereby indicating metastability and the existence of energy barriers.

To understand this hysteresis behavior, one should consider the intermediate state that can exist between the insulator and metallic phase domains and that should have a higher energy.[35] In particular, the higher energy can arise from epitaxy dislocations. Below, we outline our qualitative understanding of such metastability by using an order parameter phase field model. Consider a vector order parameter field, $\vec{\psi}(x)$, in which the components of $\vec{\psi}$ are all the relevant parameters such as a and D, and the phase indicator parameter, whose value can denote the insulator or the metallic phase. Here, x is the coordinate along the nanowire axis. In this formulation, the different states of the nanowire exhibited during the heating and cooling processes can be specified by the vector phase field order parameter. The fact that the state can no longer be characterized by a single scalar order parameter is clear: At each temperature of the transition regime, the state of the nanowire is not spatially homogeneous and requires a multivalued, spatially varying description. This can be precisely provided by the vector field $\vec{\psi}(x)$. In addition, if we specify a Ginzburg–Landau type of free energy as a functional of $\vec{\psi}(x)$, that is, $f|\vec{\psi}(x)|$, then the states observed during the heating and cooling processes must be located at the local free energy minima in this multidimensional functional landscape, separated by an energy barrier. In terms of a "path" in this functional space connecting the two local minima, one can always identify one that has the lowest energy barrier, generally denoted the minimum energy path (MEP), for example, by using the string method.[36,37] Denoting the generalized coordinate of such path by s, we illustrate the phase-transition process of the nanowire in Figure 6. In Figure 6A, we show the free energy of the two states at the point when both are at the same free energy, which perhaps happens at around a temperature intermediate between the maximum and the minimum, that is, around 80 °C. In Figure 6B, we give an overall picture of the transition process as indicated by the solid line with arrows (showing the direction of temperature variation). Metastability and asymmetry of the heating and cooling processes are clearly an outgrowth of the energy barrier that separates the two states. That is, during heating, since the initial state is the insulating state, it will be at the right-hand-side minimum of the free energy in Figure 6B until the barrier disappears at the upper limit of the transition regime, at which point the state slides into the minimum on the left-hand-side of the free energy in Figure 6B. When cooling, the state remains in this continuously evolving minimum state until the lower limit of the transition regime, at which point the state slides into the minimum on the right-hand-side, and the cycle is thus complete.

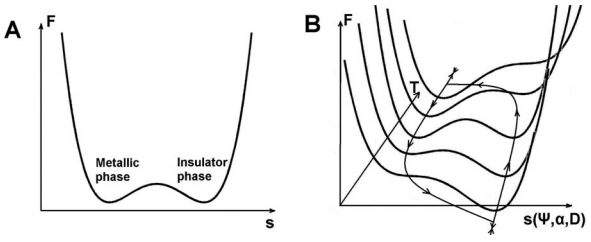

Figure 6. A schematic illustration of the free energy functional plotted as a function of the minimum energy path parameter *s*. (A) The free energy landscape along the MEP at a temperature where the heating and cooling states have the same free energy, perhaps at around 80 °C. Here the minimum on the left side is the state that is initially metallic, whereas the minimum on the right is initially insulating. (B) An illustration of the hysteresis loop with its corresponding free energy landscape as depicted by the MEP. The arrows indicate the direction of temperature variation.

Associated with the hysteresis behavior is the variation of the average metallic fraction in the domains, which was observed to be: $a_0^{\text{real}} < a_0$ in the heating process, and $a_0^{\text{real}} > a_0$ in the cooling process. This behavior is reflected in the resistance of our nanowire system shown in Figure 4B. The metallic phase of VO_2 is a conductor, and in the periodic polydomain structure, the total resistance can be regarded as a series connection of the conducting (metallic phase) and semiconducting (insulator phase) spatial regions. Similar to the derivation by Wei et al.,[38] if the metallic parts have essentially zero electric resistance and the semiconducting parts have electrical resistivity ρ, then the total resistance can be given by Equation (5).

$$R = \frac{1}{S}\Sigma D(1-\alpha)\rho = \frac{L\rho}{S}(1-\alpha) \tag{5}$$

where L is the length of the nanowire and S is its cross-sectional area. So the hysteresis behavior in a is reflected in measured resistance. In our experiment, the resistance during the heating process is larger than that during the cooling process, which is totally consistent with the prediction of Equation (5) together with the observed variation of a. At high temperatures, there is a sudden transition whereby the polydomain structure changes into a single-domain metallic phase, concurrent with a sudden change in a.

The hysteresis behavior in polydomain structure parameters (a and D), shown in Figure 5B, can also be qualitatively understood under the above considerations. It is important to note that the starting points of heating and cooling processes are different. In the heating process, the starting point is at $a = 0$, $D = \infty$. New domains appear in the nanowire one by one; and this "domain insertion" refers to the increase of the metallic percentage concurrent with the decrease of polydomain period D, until a exceeds approximately 0.5, when the entire nanowire turns into the metallic phase. This evolutionary path is qualitatively consistent with the prediction of Equation (3), because other paths

have higher free energy. For example, it is difficult to increase α alone without changing D. Around the starting point of the heating process (D large), the term $\xi\alpha^2(1-\alpha)^2$-De^I from Equation (1) is very important when D is large. Hence "domain insertion" behavior is the favored evolutionary path to decrease the free energy. However, during the cooling process, the starting point is initially set to the starting point $\alpha \approx 1/2$, $D \approx 4\sqrt{2\gamma h/\xi e^I}$, with the sudden appearance of polydomain structure at around 95–100 °C. Cooling causes the system to evolve along another path, in which α characteristically decreases and D remains unchanged. This might be understood by noting the fact that around the starting point, over a wide range of α values, the change in the equilibrium period, D_0, is quite small (see Figure 7). When this is coupled with the existence of an energy barrier, it is easy to see that the change in D is blocked.

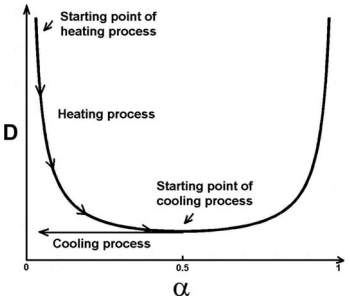

Figure 7. A two-dimensional plot of the free energy minimum, in accordance with Equation (3), as a function of α and D. Together with the increase in α, D is noted to decrease. In both heating and cooling processes, the evolutionary paths of the system are different. They are labeled in the figure by arrows. Around $\alpha \approx 0.5$, the change in D_0 is quite small, and due to the existence of the energy barrier, the evolution path in the cooling process tends to preserve D_0.

The reason why there is a sudden appearance of polydomain structure in the cooling process, with an initial $\alpha \approx 1/2$, is still not very clear and needs further investigation. The observed behavior hints that it may be a spinodal decomposition process, or periodic nucleation caused by epitaxial growth. Although in a structural phase transition, the spinodal decomposition mechanism will induce a $k = 0$ exponential growth mode as predicted by the Landau–Khalatnikov (LK) model,[39] the existence of VO_2–substrate interaction may introduce a fourth-order gradient term in the free energy equation of the LK model, and this term can induce a nonzero spatial wave vector for the fastest growth mode in the spinodal decomposition process, thereby leading to a polydomain structure. Such a direction of investigation is presently being pursued.

Conclusions

VO_2 nanowires exhibited excellent in-plane epitaxial growth along three equivalent $<1\bar{1}00>$ directions of the C-planes of the sapphire substrates. The crystallographic growth direction of these nanowires was along the [100] direction of the VO_2 monoclinic structure. VO_2 nanowires often formed V-shaped bicrystal nanostructures at a relatively low growth temperature. For the MIT properties of individual VO_2 nanowires, we observed that the sharp electrical hysteresis loops of the single VO_2 nanowire were altered dramatically by the interface elastic strain. Because of the interface energy, distinct periodic domain structures appeared in the "grown nanowires". Such a domain structure can be partially explained under the framework of a modified stress-induced elastic energy model that was initially developed for ferroelectric systems. The "grown nanowire devices" had a much broader transition temperature range than did the "dispersed devices" due to the formation of the periodic domain structures. VO_2 nanowire structures grown along the substrate surface demonstrated advantages in device fabrication. They have great potential to be used in the fabrication of complex structures in nanodevices.

Experimental Section

VO_2 nanowires were grown by a simple chemical vapor deposition (CVD) method without using any metal catalysts.[18] VO_2(B) powders (purity 99.9%, Aldrich) were used as the source material, which were loaded into an alumina boat and placed at the center zone of a tube furnace. Sapphire substrates were cleaned by using a standard wafer cleaning procedure and were placed at a fixed distance (about 1 cm) from the crucible. Before heating the source material, the furnace tube was evacuated to about 10^{-3} Torr. Then, the furnace temperature was increased at a rate of 10 °C/min and finally maintained at about 900 °C for 2 h.

For the growth of free-standing VO_2 nanowires, an R-plane sapphire substrate was used. The VO_2 nanowires were grown on the C-plane and R-plane sapphire substrates at the same time in the tube furnace. The free-standing VO_2 nanowires grown on the R-plane substrate were collected by two methods. (1) By scratching, some VO_2 nanowires fell directly on the substrate surface (or on carbon supporting films for characterization by electron microscopy). (2) The VO_2 nanowires were ultrasonicated and dispersed in an alcohol solution. The resulting nanowire suspension was then dropped onto the sapphire substrate for electron-beam lithography. The scratching method can effectively minimize surface contamination of the nanowires; however, our high-resolution electron microscopy study showed that the surfaces of the VO_2 nanowires collected by these two methods were not contaminated, and no defects were introduced.

The morphology of the VO_2 nanowires was studied with a JEOL-6700 field-emission scanning electron microscope (SEM). The nanowire structure was investigated with a Philips CM 120 analytical transmission electron microscope (TEM) and a high-resolution JEOL-2010F TEM. The electrical contacts attached onto the individual nanowires were fabricated by the standard electron-beam lithography (EBL) process. C-plane sapphire substrates were first photolithographically patterned with Ti (20 nm)/Au (70 nm) "micro patterns". Free-standing VO_2 nanowires were collected and dispersed onto the sapphire substrate surface. The VO_2 nanowires directly grown on the C-plane sapphire and the VO_2 nanowires simply dispersed on the sapphire substrate were both coated with PMMA poly(methyl methacrylate), followed by EBL and the thermal evaporation of the Cr (20 nm)/Au (100 nm) film as the electri-

cal contacts on the nanowires. The electrical properties of the nanowires were measured by using a semiconductor parameter analyzer (HP 4156B) with a wafer probe station equipped with a home-made hot stage.

Acknowledgments

The authors are grateful to Prof. Ping Sheng for helpful discussions. This work was supported by the Research Grants Council of Hong Kong (Project Nos. CityU5/CRF/08, 603408, and HKUST9/CRF/08).

[1] J. I. Sohn, H. J. Joo, A. E. Porter, C. J. Choi, K. Kim, D. J. Kang, M. E. Welland, *Nano Lett.* **2007**, *7*, 1570–1574.
[2] F. J. Morin, *Phys. Rev. Lett.* **1959**, *3*, 34–36.
[3] L. K. Elbaum, M. N. Newns, H. Zeng, V. Dericke, J. Z. Sun, R. Sandstorm, *Nature* **2004**, *431*, 672–676.
[4] E. Vailova, I. Hellmann, V. Kataev, C. Taschner, B. Buchner, R. Klingeler, *Phys. Rev. B* **2006**, *73*, p144417.
[5] S. Biermann, A. Poteryaev, A. I. Lichtenstein, A. Georges, *Phys. Rev. Lett.* **2005**, *94*, p0246404.
[6] M. M. Qazilbash, M. Brehm, B.-G. Chae, P.-C. Ho, G. O. Andreev, B.-J. Kim, S. J. Yun, A. V. Balatsky, M. B. Maple, F. Keilmann, H.-T. Kim, D. N. Basov, *Science* **2007**, *318*, 1750–1753.
[7] X. D. Wang, C. J. Summers, Z. L. Wang, *Nano Lett.* **2004**, *4*, 423–426.
[8] B. Nikoobakht, *Chem. Mater.* **2007**, *19*, 5279–5284.
[9] B. Nikoobakht, C. A. Michaels, S. J. Stranick, M. D. Vaudin, *Appl. Phys. Lett.* **2004**, *85*, 3244–3246.
[10] B. H. Hong, S. C. Bae, C.-W. Lee, S. Jeong, K. S. Kim, *Science* **2001**, *294*, 348–351.
[11] Y. F. Gao, M. Nagai, T.-C. Chang, J.-J. Shyue, *Cryst. Growth Des.* **2007**, *7*, 2467–2471.
[12] L. E. Greene, M. Law, J. Goldberger, F. Kim, J. C. Johnson, Y. F. Zhang, R. J. Saykally, P. D. Yang, *Angew. Chem. Int. Ed.* **2003**, *42*, 3031–3034.
[13] P. A. Smith, C. D. Nordquist, T. N. Jackson, T. S. Mayer, B. R. Martin, J. Mbindyo, T. E. Mallouk, *Appl. Phys. Lett.* **2000**, *77*, 1399–1401.
[14] J. Li, C. Papadopoulos, J. M. Xu, *Appl. Phys. Lett.* **1999**, *75*, 367–369.
[15] S. Fan, M. G. Chapline, N. R. Franklin, T. W. Tombler, A. M. Cassell, H. Dai, *Science* **1999**, *283*, 512–514.
[16] J. S. Speck, A. C. Daykin, A. Seifert, A. E. Romanov, W. Pompe, *J. Appl. Phys.* **1995**, *78*, 1696–1706.
[17] W. D. Nix, B. M. Clemens, *J. Mater. Res.* **1999**, *14*, 3467–3473.
[18] Y. Cheng, T. L. Wong, K. M. Ho, N. Wang, *J. Cryst. Growth* **2009**, *311*, 1571–1575.
[19] B. S. Guiton, Q. Gu, A. L. Prieto, M. S. Gudiksen, H. K. Park, *J. Am. Chem. Soc.* **2005**, *127*, 498–499.
[20] J. F. De Natale, P. J. Hood, A. B. Harker, *J. Appl. Phys.* **1989**, *66*, 5844–5850.
[21] L. A. Gea, J. D. Budai, L. A. Boatner, *J. Mater. Res.* **1999**, *14*, 2602–2610.
[22] P. Jin, K. Yoshimura, S. Tanemura, *J. Vac. Sci. Technol.* **1997**, *15*, 1113–1117.
[23] J. Q. Wu, Q. Gu, B. S. Guiton, N. P. de Leon, L. Ouyang, H. K. Park, *Nano Lett.* **2006**, *6*, 2313–2317.
[24] A. Haras, M. Witko, D. R. Salahub, K. Hermann, R. Tokarz, *Surf. Sci.* **2001**, *491*, 77–87.
[25] B. S. Kwak, A. Erbil, B. J. Wikens, J. D. Budai, M. F. Chisholm, L. A. Boatner, *Phys. Rev. Lett.* **1992**, *68*, 3733–3736.
[26] J. S. Speck, W. Pompe, *J. Appl. Phys.* **1994**, *76*, 466–476.
[27] A. L. Roytburd, *J. Appl. Phys.* **1998**, *83*, 239–245.
[28] B. Fisher, *J. Phys. C: Solid State Phys.* **1975**, *8*, 2072–2076.
[29] B. Fisher, *J. Phys. C: Solid State Phys.* **1976**, *9*, 1201–1209.
[30] V. I. Emelyanov, A. L. Semenov, *Sov. Phys. Solid State* **1990**, *32*, 1790–1792.
[31] K. A. Valiev, V. G. Mokerov, V. V. Saraikin, A. G. Petrova, *Sov. Phys. Solid State* **1977**, *19*, 1487–1491.
[32] J. Dho, Y. N. Kim, Y. S. Hwang, J. C. Kim, N. H. Hur, *Appl. Phys. Lett.* **2003**, *82*, 1434–1436.
[33] J. B. Goodenough, *J. Solid State Chem.* **1971**, *3*, 490–500.
[34] A. L. Roytburd, *J. Appl. Phys.* **1998**, *83*, 228–245.
[35] D. Raquet, P. Leroux-Hugon, *Phys. Rev. B* **1980**, *22*, 5284–5301.
[36] E. Weinan, W. Ren, E. Vanden-Eijnden, *Phys. Rev. B* **2002**, *66*, 052301 (4 pp).
[37] E. Weinan, W. Ren, E. Vanden-Eijnden, *J. Appl. Phys.* **2003**, *93*, 2275–2282.
[38] J. Wei, Z. H. Wang, W. Chen, D. H. Cobden, *Nat. Nanotechnol.* **2009**, *4*, 420–424.
[39] S. B. Goryachev, *Phys. Rev. Lett.* **1994**, *72*, 1850–1853.

Received: April 29, 2010
Published Online: August 24, 2010

